

# Full One-loop Calculation of Neutralino Annihilation Into Two Photons

Lars Bergström\*

Department of Physics, Stockholm University,  
Box 6730, SE-113 85 Stockholm, Sweden

Piero Ullio†

Department of Theoretical Physics, Uppsala University,  
Box 803, SE-751 08 Uppsala, Sweden

June 3, 1997

## Abstract

For the first time, a full one-loop calculation of the process  $\chi\chi \rightarrow 2\gamma$  is performed, where  $\chi$  is the lightest neutralino in the minimal supersymmetric extension of the Standard Model. This process is of interest for dark matter detection, since it would give a sharp  $\gamma$  ray line with  $E_\gamma = m_\chi$ . We improve upon and correct published formulas, and give cross sections for supersymmetric models with  $\chi$  masses between 30 GeV and several TeV. We find a new contribution, previously neglected, which enhances the  $2\gamma$  rate for TeV higgsinos by up to an order of magnitude. As a byproduct, we obtain a new expression for the related process  $\chi\chi \rightarrow 2 \text{ gluons}$ , which on the other hand is generally smaller than previously calculated.

There has been a recent claim that evidence for a 3.5 TeV higgsino annihilating into a  $\gamma$  line may already exist from balloon emulsion and Air Cherenkov Telescope data. We comment on attractive features and problems with this interpretation.

---

\*lbe@physto.se

†piero@teorfys.uu.se



# 1 Introduction

Most extensions of the Standard Model of particle physics contain supersymmetry in one or another form. In particular, if gravity is unified with the other fundamental forces, it seems that supersymmetry is a necessary ingredient. The known particles of nature seem to be unstable, with very few exceptions. Of course, the stable ones have a specific significance since they have survived since the times immediately following the Big Bang, and today form the visible structures (clusters, galaxies, stars, planets . . .) in the Universe.

If there exist stable particles in the supersymmetric sector, those should also have survived, and could give a contribution to the total mass density of the Universe in a way which is calculable once the supersymmetric model is specified. Models which could contain stable particles are usually endowed with a symmetry,  $R$ -parity, which guarantees that the lightest supersymmetric particle is stable (for a review, see [1]). If this particle is electrically neutral, as is the case for the neutralino (a linear combination of the superpartners of the photon, the  $Z$  boson and two neutral  $CP$ -even Higgs bosons), its weak interaction strength provides a relic density which can be within an order of magnitude of the critical density of the Universe,

$$\rho_{crit} = 1.9 \cdot 10^{-29} h^2 \text{ g/cm}^3, \quad (1)$$

where  $h$  is the Hubble parameter in units of  $100 \text{ km s}^{-1} \text{ Mpc}^{-1}$ . Present measurements [2, 3] indicate that  $h$  is in the range  $0.5 - 0.7$ . It is customary when discussing energy density to normalize to the critical density through the dimensionless quantity  $\Omega$ :

$$\Omega = \frac{\rho}{\rho_{crit}}. \quad (2)$$

With the present value of  $h$ , the critical density  $\Omega = 1$  corresponds to  $\Omega h^2 = 0.25 - 0.5$ .

From dynamical estimates of the total mass density on cluster and supercluster scales, it is found that  $\Omega_{tot} > 0.4$  [4]. An analysis based on supernovas of type Ia as standard candles [5] is not inconsistent with  $\Omega = 1$ , a value which has a strong theoretical preference since it is predicted in generic models of inflation. The contribution  $\Omega_b$  from ordinary matter (mainly baryons) is limited by nucleosynthesis arguments to be less than around 0.1 [6]. Also, structure formation from the primordial fluctuations seen in the microwave background seems to be problematic unless there is a considerable amount of dark matter [7].

The “missing mass” problem found in the analysis of galactic rotation curves [8] may thus have as its solution the existence of a relic population of neutral massive particles residing in the galactic halos. We will assume that these particles are neutralinos  $\chi \equiv \tilde{\chi}_1^0$ , the lightest supersymmetric particle in the minimal supersymmetric extension of the Standard Model.

# 2 Detection methods

Several methods have been discussed to detect neutralinos (for a comprehensive list of reference for all methods mentioned here, see [1]). One possibility is to register scattering of neutralinos directly in sensitive terrestrial detectors, well shielded from radioactive and other backgrounds. After several years of development, some of these experiments now have a sensitivity large enough to rule out some supersymmetric models which otherwise satisfy all accelerator and other constraints [9, 10].



Other, more indirect, methods utilize the fact that neutralinos in the halo (or those accumulated gravitationally in massive bodies like the Earth and the Sun) may annihilate, resulting in ordinary particles which may be detected. For example, antiprotons and positrons which are not produced in large quantities by cosmic rays, would be produced in annihilations in the halo and would be continuously injected and “stored” during around  $10^7$  years which is the containment time of cosmic rays in the galaxy. Although the fluxes could be of measurable size the problem is that they are generally not much larger than the cosmic-ray induced fluxes, which necessitates a difficult model-dependent background subtraction. Also, since the spatial and energy distributions of these antiparticles are rather featureless, the lack of definitive signature is a problem. This is also true for annihilation into particles which give secondary gamma rays. Although this could give a broad feature in the spectrum up to the neutralino mass, it is in most supersymmetric models too weak to be convincing [11].

A much better signature is given by neutralino annihilation into neutrinos near the centre of the Earth or the Sun. Since the ordinary solar neutrinos only have at most MeV energies, a multi-GeV neutrino signal from the Sun (or the Earth) would be an unmistakable signal. If the neutrino detector has an angular resolution better than a few degrees, the mass of the annihilating particles can be determined with reasonable accuracy [12]. Also this method has already given useful constraints on supersymmetric models of dark matter [13], and has a large future potential as large new neutrino telescopes are being built [14].

Finally, an excellent signature is provided by the annihilation of neutralinos in the halo into two-body final states containing a photon, such as  $\gamma\gamma$ . This process was first proposed by Bergström and Snellman [15], who also first estimated the related two-gluon process (for photinos). Other early references include [16, 17, 18]. Since the annihilating neutralinos move with galactic velocities,  $v/c \sim 10^{-3}$ , the result is a gamma ray line of phenomenal peak-to-width ratio. This signature has no conceivable background from known astrophysical sources. To optimally utilize this sharp signal peak, detectors with energy resolution at the percent level and below should ideally be used. In the region 30 - 100 GeV, where “light” neutralinos (mostly rather pure binos) are likely to reside, a detector has to be placed in orbit (above the atmosphere) not to be flooded with cosmic-ray produced atmospheric gammas. This led to a (temporary?) impasse for this idea, since photon detectors with high energy resolution are generally very heavy and therefore costly to launch.

It was subsequently realised, in work by Urban et al [19], that a certain type of ground-based detector (Air Cherenkov Telescopes, ACT) could be used for searching for gamma lines from very heavy neutralinos (several hundred GeV to the TeV region). Here the limited energy resolution (10 %, at best) is partly offset by the very large collection areas possible ( $10^4$  to  $10^5$  m<sup>2</sup>). The rates for TeV neutralinos (generally higgsinos, since binos of such masses would overclose the Universe) were calculated in [20]. In this paper, the process  $\chi\chi \rightarrow Z\gamma$  was also proposed as an important channel, and a lower bound based on unitarity for high-mass higgsino annihilation into  $\gamma\gamma$  and  $Z\gamma$  was computed. In [21], a more complete calculation of the  $\gamma\gamma$  process was presented, and the phenomenology was also worked out in [22] (although in none of these TeV neutralinos were considered).

Since there is a new generation of Air Cherenkov telescopes being planned [23], and also a new ambitious satellite project [24], we have considered it timely to revisit the  $\gamma\gamma$  process, performing for the first time a full one-loop calculation improving on the estimates of previous work. As a byproduct, we also recompute the two-gluon process, correcting a numerically significant error in [25]. We give analytical expressions for all the amplitudes and give results



of scans in supersymmetric parameter space for several sets of models.

During the final stages of this work, we have come upon a recent paper [26], where it is claimed that evidence for a TeV higgsino annihilating into a  $\gamma$  line may already exist from balloon emulsion and ACT data. We will comment on attractive features and problems with this interpretation.

It is important to note that all the different methods to detect supersymmetric dark matter are complementary in many respects. Each process has certain regions in parameter space where it dominates. In fact, for TeV higgsinos, the  $\gamma$  line process may probe supersymmetric models out of reach for accelerators in the foreseeable future (for other possible methods to detect heavy higgsinos, see [27]).

### 3 Cross section

We compute the full expression for the annihilation cross section of the process

$$\tilde{\chi}_1^0 + \tilde{\chi}_1^0 \rightarrow \gamma + \gamma \quad (3)$$

in the limit of vanishing relative velocity of the neutralino pair. This result can be applied to neutralinos annihilating in the galactic halo, where it is estimated that massive dark matter particles move with a velocity of the order  $v/c \sim 10^{-3}$ . The outgoing photons will then be nearly monochromatic, with an energy equal to the mass of  $\tilde{\chi}_1^0$ . Furthermore, for very low relative velocity, the neutralino pair must be in a S wave state with pseudoscalar quantum numbers; we can therefore project out of the amplitude the  $^1S_0$  state, using the projector [28]

$$\mathcal{O}_{Ps} = -\frac{M_\chi}{\sqrt{2}} \gamma^5 \left( 1 - \frac{\not{p}}{M_\chi} \right) \quad (4)$$

where  $M_\chi$  is the mass of  $\tilde{\chi}_1^0$  and  $p = (M_\chi, \vec{0})$  its momentum. Analyzing the Dirac structure of the Feynman diagrams we can draw for this process, we can exclude a priori those diagrams which cannot generate a pseudoscalar state.

As suggested in Ref. [20], it is convenient to compute the W boson and unphysical Higgs loop diagrams choosing the non linear gauge defined in Ref. [29], which is a slight variant of the usual linear R-gauge (or 't Hooft gauge). In this particular gauge the  $W^\pm G^\mp \gamma$  vertex vanishes and some of the box diagrams which, in the linear R-gauge, may give a contribution to the amplitude are not present. In addition the  $W^\pm W^\mp \gamma$  vertex and the W propagator assume simpler forms. We find that the Feynman diagrams we have to include in the computation, at one loop level, are those shown in Fig. 1.

There is another property that introduces a further main simplification. In any process of annihilation of particles at rest, the four point loop integrals one obtain from each box diagram applying the Feynman rules, can always be rewritten as a linear combination of three-point integrals. This is possible because, for each integral, one can find a linear combination of the four factors in the denominator which is independent of the momentum flowing in the loop. It follows that we do not have any four-point integral in the computation of the amplitude.



The amplitude of the annihilation process can be factorized in the form

$$\mathcal{A} = \frac{e^2}{2\sqrt{2}\pi^2} \epsilon(\epsilon_1, \epsilon_2, k_1, k_2) \tilde{\mathcal{A}} \quad (5)$$

where  $\epsilon_1, \epsilon_2$  and  $k_1, k_2$  are respectively the polarization tensors and the momenta of the two outgoing photons. The cross section is then given, as a function of  $\tilde{\mathcal{A}}$ , by the formula

$$v\sigma_{2\gamma} = \frac{\alpha^2 M_\chi^2}{16\pi^3} \left| \tilde{\mathcal{A}} \right|^2. \quad (6)$$

We write the total amplitude as the sum of the contributions obtained from the four different classes of diagrams:

$$\tilde{\mathcal{A}} = \tilde{\mathcal{A}}_{f\bar{f}} + \tilde{\mathcal{A}}_{H^+} + \tilde{\mathcal{A}}_W + \tilde{\mathcal{A}}_G.$$

The single contributions are listed below. In each of them we separate real and imaginary parts. To facilitate a comparison, we follow as closely as possible the notation of [21].

1) Contribution of the fermion-sfermion loop diagrams (1a-1d in Fig. 1). The sum over  $f$  includes the quarks and the charged leptons, the sum over  $\tilde{f}$  the corresponding sfermion in both chiral states.

$$\begin{aligned} \text{Re } \tilde{\mathcal{A}}_{f\bar{f}} &= \sum_{f\bar{f}} c_f \frac{e_f^2}{M_\chi^2} \left[ \frac{1}{2} \frac{b S_{f\bar{f}} + \sqrt{a} b D_{f\bar{f}}}{1+a-b} I_1(a, b) + \frac{1}{2} \frac{S_{f\bar{f}}}{1-b} I_2(a, b) \right. \\ &\quad \left. + \left( \frac{b S_{f\bar{f}} + \sqrt{a} b D_{f\bar{f}}}{1+a-b} - \frac{1}{2} \frac{b S_{f\bar{f}}}{1-b} \right) I_3(a, b) \right] \\ &\quad + \sum_f c_f \frac{e_f^2}{M_\chi^2} \left[ \left( \frac{m_f^2 G_{Zf}}{4 m_Z^2} - \frac{m_f M_\chi G_{H_3^0 f}}{4 (4 M_\chi^2 - m_{H_3^0}^2)} \right) I_1(a, b) \right] \end{aligned} \quad (7)$$

$$\begin{aligned} \text{Im } \tilde{\mathcal{A}}_{f\bar{f}} &= -\pi \sum_f c_f \frac{e_f^2}{M_\chi^2} \left[ \sum_{\tilde{f}} \left( \frac{1}{2} \frac{b S_{f\bar{f}} + \sqrt{a} b D_{f\bar{f}}}{1+a-b} \right) + \frac{m_f^2 G_{Zf}}{4 m_Z^2} \right. \\ &\quad \left. - \frac{m_f M_\chi G_{H_3^0 f}}{4 (4 M_\chi^2 - m_{H_3^0}^2)} \right] \cdot \log \left( \frac{1 + \sqrt{1-b/a}}{1 - \sqrt{1-b/a}} \right) \theta(1 - m_f^2 / M_\chi^2) \end{aligned} \quad (8)$$

where  $m_Z$  and  $m_{H_3^0}$  are the masses of the Z boson and of the Higgs pseudoscalar  $H_3^0$ , and we have defined:

$$a = \frac{M_\chi^2}{M_{\tilde{f}}^2} \quad b = \frac{m_f^2}{M_{\tilde{f}}^2}$$

$$S_{f\bar{f}} = \frac{1}{2} \left( g_{f\bar{f}1}^L g_{f\bar{f}1}^{L*} + g_{f\bar{f}1}^R g_{f\bar{f}1}^{R*} \right) \quad D_{f\bar{f}} = \frac{1}{2} \left( g_{f\bar{f}1}^L g_{f\bar{f}1}^{R*} + g_{f\bar{f}1}^R g_{f\bar{f}1}^{L*} \right)$$



$$G_{Zf} = \frac{g T_f^3}{\cos \theta_W} (g_{Z11}^L - g_{Z11}^R) \quad G_{H_3^0 f} = (g_{H_3^0 11}^R - g_{H_3^0 11}^L) (g_{H_3^0 ff}^L - g_{H_3^0 ff}^R) \quad .$$

The index 1 is referred to  $\tilde{\chi}_1^0$ ,  $e_f$  is the charge of the fermion in unit of the electron charge ( $-e$ ),  $c_f$  is the color factor equal to 3 for quarks and to 1 for leptons,  $T_f^3$  is the third component of the weak isospin equal to  $+1/2$  for  $f=u,c,t$  and to  $-1/2$  for  $f=e,\mu,\tau,d,s,b$ .

2) Contribution of the chargino-Higgs boson loop diagrams (2a-2d in Fig. 1). The sum over  $\chi_i^+$  includes the two chargino eigenstates.

$$\begin{aligned} Re \tilde{\mathcal{A}}_{H^+} = & \sum_{\chi_i^+} \frac{1}{M_\chi^2} \left[ \frac{1}{2} \frac{b S_{\chi H} + \sqrt{a} b D_{\chi H}}{1 + a - b} I_1(a, b) + \frac{1}{2} \frac{S_{\chi H}}{1 - b} I_2(a, b) \right. \\ & + \left( \frac{b S_{\chi H} + \sqrt{a} b D_{\chi H}}{1 + a - b} - \frac{1}{2} \frac{b S_{\chi H}}{1 - b} \right) I_3(a, b) \\ & \left. + \left( \frac{M_{\chi_i^+}^2 G_{Z\chi}}{4 m_Z^2} - \frac{M_{\chi_i^+} M_\chi G_{H_3^0 \chi}}{4 (4 M_\chi^2 - m_{H_3^0}^2)} \right) I_1(a, b) \right] \end{aligned} \quad (9)$$

$$Im \tilde{\mathcal{A}}_{H^+} = 0 \quad (10)$$

where we have defined:

$$a = \frac{M_\chi^2}{m_{H^+}^2} \quad b = \frac{M_{\chi_i^+}^2}{m_{H^+}^2}$$

$$S_{\chi H} = \frac{1}{2} (g_{H^+ 1i}^L g_{H^+ 1i}^{L*} + g_{H^+ 1i}^R g_{H^+ 1i}^{R*}) \quad D_{\chi H} = \frac{1}{2} (g_{H^+ 1i}^L g_{H^+ 1i}^{R*} + g_{H^+ 1i}^R g_{H^+ 1i}^{L*})$$

$$G_{Z\chi} = (g_{Zii}^R - g_{Zii}^L) (g_{Z11}^L - g_{Z11}^R) \quad G_{H_3^0 \chi} = (g_{H_3^0 11}^R - g_{H_3^0 11}^L) (g_{H_3^0 ii}^L - g_{H_3^0 ii}^R)$$

and the index i is referred to  $\tilde{\chi}_i^+$ .

3) Contribution of the chargino-W boson loop diagrams (3a-3c in Fig. 1).

$$\begin{aligned} Re \tilde{\mathcal{A}}_W = & \sum_{\chi_i^+} \frac{1}{M_\chi^2} \left[ 2 \frac{(a-b) S_{\chi W}}{1 + a - b} I_1(a, b) + \frac{S_{\chi W} - 2\sqrt{a} D_{\chi W}}{1 - a - b} I_1(a, 1) \right. \\ & + \left( 2 \frac{S_{\chi W} - 2\sqrt{a} D_{\chi W}}{1 - a - b} - \frac{3 S_{\chi W} - 4\sqrt{a} D_{\chi W}}{1 - b} \right) I_2(a, b) \\ & \left. + \left( \frac{(2+b) S_{\chi W} - 4\sqrt{a} D_{\chi W}}{1 - b} - 2 \frac{(1-a+b) S_{\chi W}}{1 + a - b} \right) I_3(a, b) \right] \end{aligned} \quad (11)$$

$$Im \tilde{\mathcal{A}}_W = -\pi \sum_{\chi_i^+} \frac{1}{M_\chi^2} \left( 2 \frac{(a-b) S_{\chi W}}{1 + a - b} \right).$$



$$\cdot \log \left( \frac{1 + \sqrt{1 - b/a}}{1 - \sqrt{1 - b/a}} \right) \theta (1 - m_W^2 / M_\chi^2) \quad (12)$$

where in this case:

$$a = \frac{M_{\chi_1^0}^2}{M_{\chi_i^+}^2} \quad b = \frac{m_W^2}{M_{\chi_i^+}^2}$$

$$S_{\chi W} = \frac{1}{2} (g_{W1i}^L g_{W1i}^{L*} + g_{W1i}^R g_{W1i}^{R*}) \quad D_{\chi W} = \frac{1}{2} (g_{W1i}^L g_{W1i}^{R*} + g_{W1i}^R g_{W1i}^{L*}) \quad .$$

4) Contribution of the chargino-unphysical Higgs loop diagrams (4a-4b in Fig. 1).

$$\begin{aligned} Re \tilde{\mathcal{A}}_G &= \sum_{\chi_i^+} \frac{1}{M_\chi^2} \left[ -\frac{1}{2} \frac{S_{G\chi} + \sqrt{a} D_{G\chi}}{1 - a - b} I_1(a, 1) \right. \\ &\quad \left. + \left( \frac{1}{2} \frac{S_{G\chi}}{1 - b} - \frac{S_{G\chi} + \sqrt{a} D_{G\chi}}{1 - a - b} \right) I_2(a, b) - \frac{1}{2} \frac{b S_{G\chi}}{1 - b} I_3(a, b) \right] \end{aligned} \quad (13)$$

$$Im \tilde{\mathcal{A}}_G = 0 \quad (14)$$

where a and b are the same as those defined for the chargino-W boson contribution and

$$S_{G\chi} = \frac{1}{2} (g_{G1i}^L g_{G1i}^{L*} + g_{G1i}^R g_{G1i}^{R*}) \quad D_{G\chi} = \frac{1}{2} (g_{G1i}^L g_{G1i}^{R*} + g_{G1i}^R g_{G1i}^{L*}) \quad .$$

The coupling constants for left and right chiral states,  $g^L$  and  $g^R$ , are written in the notation adopted in the PhD Thesis of Edsjö [30]; all of them are defined therein, with the exception of the unphysical Higgs couplings, which we rewrite from Ref. [31] in the conventions of [30]:

$$g_{G1i}^L = -g \sin \beta \left[ Z_{14}^* V_{i1}^* + \sqrt{\frac{1}{2}} (Z_{12}^* + Z_{11}^* \tan \theta_W) V_{i2}^* \right] \quad (15)$$

$$g_{G1i}^R = +g \cos \beta \left[ Z_{13} U_{i1} - \sqrt{\frac{1}{2}} (Z_{12} + Z_{11} \tan \theta_W) U_{i2} \right] \varepsilon_i \quad (16)$$

The functions  $I_1(a, b)$ ,  $I_2(a, b)$  and  $I_3(a, b)$ , which arise from the loop integrations, are specified in Appendix A.  $I_1(a, b)$  is the well known three point function that appears in triangle diagrams; it is an analytic function of a/b.  $I_2(a, b)$  and  $I_3(a, b)$  are given both in form of integrals over a Feynman parameter x, and may be expressed in terms of dilogarithms. It is numerically very easy to compute them even in the integral form as, for any physically interesting value of the parameters a and b, the integrands are smooth functions of x. In the real parts there are apparently poles for  $a - b = 1$ ,  $b = 1$ ,  $a + b = 1$ : we have verified that, in each formula, a cancellation among the different contributions takes place for each of these spurious poles and therefore we do not have to deal with any numerical problem.



The results for the imaginary parts have been checked applying the Cutkosky cutting rules to the corresponding diagrams. Eq. (7) reproduces equations (2.5) in Ref. [25] and (2.5) in Ref. [21] except for one small, but numerically significant, error in both of these.\* As we will briefly sketch in Section 6 this discrepancy may have led, for some SUSY models, to an overestimate of the cross section of the annihilation of neutralinos into two gluons. In Eq. (12), fixing the overall sign through Eq. (8), we do not agree with the sign of the result quoted in Ref. [21]. This sign difference is numerically important in cases where the amplitudes are of the same order of magnitude.

## 4 Results and Discussion

We have calculated the  $\chi\chi \rightarrow 2\gamma$  rates for a broad selection of supersymmetric models. All experimental constraints on the parameters have been checked, and only non-excluded models have been treated. (For a detailed explanation of the method of computation and the parametrization of models, see [30].)

The calculation of the relic density  $\Omega h^2$  has been done using the full machinery of exact treatment of resonances and thresholds [32], loop corrections to masses and vertices [33] and coannihilations [34]. We are only interested in models which have a chance to at least explain the galactic halos, so we keep in all the graphs presented here only models which satisfy  $0.025 < \Omega h^2 < 1$ .

The detection rate of galactic gamma rays from neutralino annihilations depends on two different parts. One concerns the particle physics calculation of the  $2\gamma$  cross section for a given set of supersymmetric model parameters, and also the calculation of the relic abundance of neutralinos in standard Big Bang cosmology. The second part concerns the distribution of neutralinos in the galactic dark matter halo, which is a difficult problem of galactic structure formation. Unfortunately, all detection predictions are very sensitive to the poorly known dark matter mass distribution in the halo, since the  $\gamma$  line flux from a volume element  $dV$  of density  $\rho_\chi$  is given by

$$d\Phi_\gamma = 2 \frac{v\sigma_{2\gamma} \rho_\chi^2}{4\pi d^2 M_\chi^2} dV, \quad (17)$$

where  $d$  is the distance to the volume element and the factor of 2 comes because there are two  $\gamma$ s per annihilation. To obtain the full rate, one has to integrate this expression over all the halo (or, for a particular direction, over the line-of-sight).

We start by discussing the halo-model independent quantities, which can be used for any particular halo dark matter distributions. Later we discuss the expected rates for some examples of halo models.

In Fig. 2 we show the prediction for the annihilation rate into two photons,  $v\sigma_{2\gamma} \equiv v\sigma(\tilde{\chi}_1^0 + \tilde{\chi}_1^0 \rightarrow \gamma + \gamma)$  for a broad scan in supersymmetric parameter space (the parameter range is identical to that of the “generous scan” of Table 2.2 in [34, 30]). As can be seen, for the

---

\*In the formula (2.5) of [25], we think that the argument of the denominator of the second logarithm should be  $b - a(1 - x^2)$  instead of  $b + a(1 - x^2)$ . This is plausible on general grounds, since it is precisely the zero of this expression in the integrand which gives an imaginary part when  $m_\chi > m_f$ . It seems this error has propagated to the computer code of [1].



low-mass region the rate varies over many orders of magnitude. In the most favourable cases, it is of the order of a few times  $10^{-29} \text{ cm}^3 \text{ s}^{-1}$ , whereas it can be as low as  $10^{-6}$  of that value for other models. This wide spread of predictions is typical of supersymmetry scans also for direct detection and neutrino detection rates. Low  $2\gamma$  rates are obtained for binos and mixed neutralinos, whereas higgsinos give a larger rate. This is particularly clear at the high mass end, where the  $\Omega h^2$  requirement forces most of the allowed models to have a large higgsino fraction, and due to the  $W$  diagrams the  $2\gamma$  rate is exceptionally large for TeV higgsinos [20]. In this scan, the squark masses were generally quite large, which explains why also at low masses the models with the highest  $\gamma$  rates are mainly higgsino-like.

In Figs. 3 (a) and (b), we have made more extensive scans for the low- and high-mass regions respectively. In the low-mass case, Fig. 3 (a), we have allowed a larger fraction of models with low squark mass parameter (down to 150 GeV), since the bino rate into  $2\gamma$  is dominated by box diagrams of type (1a) and (1b). As can be seen, some models give rates of the order of  $10^{-28} \text{ cm}^3 \text{ s}^{-1}$ . Now, because of the lower squark masses, models which give the highest rates have a large gaugino component.

In the high mass region, we have focussed on the mass range between 3 and 4 TeV because of the preliminary indications in [26] of a possible signal. As can be seen, over that mass range there are many models that fulfil all accelerator and other constraints, and which all give rather high annihilation rates. The rates are in fact much higher than the lower limit, based on unitarity, given in [20] (which we reproduce). Investigating the various contributions shown in Fig. 2, we have found that the reason for the large value of the (real part of) amplitude is diagram 3c, which gives a contribution proportional to

$$\frac{1}{1 - \frac{M_{\tilde{\chi}_1^0}^2}{M_{\tilde{\chi}_i^+}^2} - \frac{m_W^2}{M_{\tilde{\chi}_i^+}^2}}.$$

In the pure higgsino limit, the lightest higgsino  $\tilde{\chi}_1^0$  and the lightest chargino  $\tilde{\chi}_1^+$  are almost degenerate, so when the neutralino is much more massive than the  $W$  boson this  $t$ -exchange graph becomes dominant. The approximate treatment in [20] only works if  $M_{\tilde{\chi}_1^0}^2 / M_{\tilde{\chi}_1^+}^2$  is much smaller than unity.

In supersymmetric models, the mass difference between  $\tilde{\chi}_1^0$  and  $\tilde{\chi}_1^+$  goes down with increasing higgsino fraction of the neutralino. Thus, the  $2\gamma$  rate should go up with decreasing gaugino fraction  $Z_g$ . This is clearly visible in Fig. 4 (a). In fact, we can approximate the pure higgsino limit  $Z_g \rightarrow 0$  by keeping only the diagrams 3a-3c and inserting  $S_W = -D_W = g_w^2/4$  ( $g_w$  is the usual weak gauge coupling constant). Doing this, we find the roughly constant value

$$v\sigma_{2\gamma}(\text{pure higgsino}) \approx 8 \cdot 10^{-28} \text{ cm}^3 \text{ s}^{-1} \quad (18)$$

over the whole range above 1 TeV.<sup>†</sup>

In Fig. 4 (b) we show the ratio

$$F_\gamma \equiv 2 \frac{v\sigma_{2\gamma}}{v\sigma_{WW}} \quad (19)$$

<sup>†</sup>Although we have not yet computed the full amplitude for  $\chi\chi \rightarrow Z\gamma$  (L. Bergström and P. Ullio, in preparation), we have checked in the same limit that that process also tends to a constant value of  $\sigma v$  - however, it is almost an order of magnitude smaller.



for our set of sampled supersymmetric models, bracketed by the unitarity lower bound of [20] and the pure higgsino rate found here. Notice the remarkable fact that a pure higgsino of 3 - 4 TeV mass can have the  $2\gamma$  channel as its dominant annihilation mode.<sup>‡</sup>

It is an interesting coincidence that a higgsino-like neutralino in the 3-4 TeV range gives a value of the relic abundance which is just right to give closure density,  $\Omega h^2 \sim 0.5$ . To arrive at this conclusion, it is essential to include in the relic abundance calculation coannihilation on the near-degenerate states, something which has only very recently been done by Edsjö and Gondolo (see Fig. 3 of [34]).

## 5 Halo models

In the most conservative model, the dark matter halo is described as an isothermal sphere with a density profile of the form:

$$\rho(r) = \rho_0 \left( \frac{a^2 + R^2}{a^2 + r^2} \right) \quad (20)$$

where  $r$  is the distance from the galactic centre,  $\rho_0 \simeq 0.3 \text{ GeV/cm}^3$  is the local halo density,  $a$  the core radius and  $R \simeq 8.5 \text{ Kpc}$  is our galactocentric distance. The gamma ray flux in a given direction is [35, 36, 37]:

$$\begin{aligned} \Phi_\gamma(\psi) &= 2 \frac{v\sigma_{2\gamma}}{4\pi M_\chi^2} \int_{\text{line of sight}} \rho^2(l) dl(\psi) \\ &\simeq 4 \cdot 10^{-10} \frac{v\sigma_{2\gamma}}{10^{-29} \text{ cm}^3 \text{ s}^{-1}} \left( \frac{10 \text{ GeV}}{M_\chi} \right)^2 J\left(\psi, \frac{R}{a}\right) \text{ cm}^{-2} \text{ s}^{-1} \text{ sr}^{-1}, \end{aligned} \quad (21)$$

where  $\psi$  is the angle between the direction of the galactic centre and that of observation. The function  $J$ , which is obtained performing analytically the integral over the line of sight, is decreasing in the interval  $[0, \pi]$  and its slope and maximum value increase as the parameter  $R/a$  increases. A typical estimate of  $J$  in the direction of the galactic centre is between  $J(0, 1/3) \sim 0.4$  and  $J(0, 2) \sim 2$ .

Several models of the galactic halo contain the hypothesis of an enhancement of the dark matter density in correspondence with the galactic centre, where there seems to be a massive nucleus. The isothermal model of Ipser and Sikivie [38], in which is predicted a large increase of the density in a region of 150 pc around the galactic centre, has been considered in Ref. [19]. The estimated flux in the direction of the galactic centre is of the order of  $10^3 \Phi_\gamma$ , where  $\Phi_\gamma \equiv \Phi_\gamma(0)$  is the flux that would result in the conservative halo model choosing  $J = 1$ , and again the value is to a large extent dependent on the parameters in the model.

In the Berezhinsky et al.[39] model, the dark matter halo density has the following profile:

$$\rho(r) = \rho_0 \left( \frac{R}{r} \right)^{1.8} \quad (22)$$

---

<sup>‡</sup>To be fully consistent, this mode should then also be included in the determination of the relic abundance. This necessitates a calculation of the momentum-dependence of the cross section, which has not been done. The effect is not expected to be dramatic. However, it implies that higgsinos could be even more massive than previously thought without overclosing the Universe.



which is assumed to be valid within 0.01 pc from the center. In this case the gamma ray source would appear pointlike with 99% of the flux emitted concentrated in a central region defined by a solid angle of less than  $10^{-5}$  sr. The flux in the direction of the galactic centre is highly enhanced, up to  $10^7 \Phi_\gamma$  [40].

An attractive hypothesis is that strings and texture fluctuations may have generated perturbations in the dark matter halo providing a clumpy density distribution [41]. Also, in standard CDM scenarios, smaller “clumps” of dark matter may merge to larger clumps like galactic halos, and some of these objects may survive tidal forces. A significant increase in the gamma ray flux can be obtained if typical  $10^8 M_\odot$  clumps are present. It is very difficult to detect such dark matter concentrations, nevertheless some of these may already have been identified, in the form of dwarf spheriodals residing in the Milky Way halo. As recently as in 1994, the Sagittarius dwarf [42] was discovered, a dwarf spheroidal that is at a distance of about 15 kpc from the centre of the Milky Way, well inside the galactic halo potential, and about 23 kpc from the Sun. It is dark matter dominated and has a density profile resembling a Heaviside function with a value of  $1.5 \text{ GeV cm}^{-3}$  on a length scale of 1 Kpc. A nice confirmation of the hypothesis of a line signal from dark matter annihilation would be the detection of an increased flux in precisely the direction of the Sagittarius dwarf. The flux in this direction would be larger by a factor of around 2 than the flux from the galactic centre. Taking the uncertainty of halo models into account, we can write the detected gamma line flux at Earth as

$$\Phi_\gamma^0 = \kappa \Phi_\gamma, \quad (23)$$

where we have seen that  $\kappa$  can vary over a large range, from around 1 to at least  $10^3$ .

In Fig. 5 we show the normalized flux  $\Phi_\gamma$  for the same models as those in Fig. 2.

It is clear that the flux reported in [26],  $\sim 10^{-9} \text{ cm}^{-2}\text{s}^{-1}\text{sr}^{-1}$ , cannot be explained by any of the scanned supersymmetric models in the conservative halo model. However, taking the pure higgsino rate (18) in the model of Berezhinsky et al, such a high flux can be obtained towards the centre of the galaxy. However, the (weaker) indications of a high flux in other directions claimed in [26] are not explicable in models where the density is only enhanced near the galactic center. A clumpy distribution with a large number of clumps rather smoothly distributed in the halo would be needed to explain the high flux of [26].

## 6 The two gluon channel

As a final application of our loop calculation, we consider the annihilation channel  $\chi\chi \rightarrow 2 \text{ gluons}$ . Here only the diagrams 1a-1d contribute, with of course no contribution from leptons. To get the cross section, one just substitutes the electric charge  $e_f^2$  with 1 in the expressions (7) and (8) above, and the colour sum and average is performed by the simple recipe [15]  $\alpha^2 \rightarrow 2\alpha_s^2$  in (6). In Fig. 6 we show the value of  $\sigma v_{2g}$  for the scan of low-mass neutralino models using our results compared to those obtained with previous formulas [25]. As can be seen, our prediction is for most of the models below the previous ones, which could make the indirect method of antiproton detection [43] more difficult than previously thought.



## 7 Conclusions

We have reinvestigated the process  $\chi\chi \rightarrow 2\gamma$  in considerable detail. Our new results supersede and correct previous partial results in the literature. A new contribution is identified, which has its main effect for heavy higgsino-like neutralinos. A TeV-scale pure higgsino may in fact have the  $2\gamma$  final state as its main annihilation mode, in addition to giving a relic density close to the critical density of the Universe.

A clumpy halo is needed, however, to explain the high rates indicated in [26] if that analysis would survive the addition of further observational data. Irrespective of the fate of that 3.5 TeV higgsino the gamma line signature is a promising one for neutralino detection and should be kept in mind when designing new gamma ray detectors. For a smooth halo, the ideal gamma ray telescope should have large collection area ( $10^4 \text{ m}^2$  or larger) and good energy resolution (down to percent level) but need not have good angular resolution. A large angular acceptance would be much more important.

As a byproduct, we have also recalculated the  $\chi\chi \rightarrow 2g$  process, where we agree with published results apart from a small, but numerically significant, difference.

## 8 Acknowledgements

We thank J. Edsjö and P. Gondolo for many discussions and for help with the numerical calculations. The work of L.B. was supported by the Swedish Natural Science Research Council (NFR).

## Appendix A

We define below the functions  $I_1(a, b)$ ,  $I_2(a, b)$  and  $I_3(a, b)$  which appear in the formulas for the real part of the amplitude. They arise from the three point loop integrals.

$$I_1(a, b) = \int_0^1 \frac{dx}{x} \log \left( \left| \frac{4ax^2 - 4ax + b}{b} \right| \right) \quad (\text{A.1})$$

$$I_2(a, b) = \int_0^1 \frac{dx}{x} \log \left( \left| \frac{-ax^2 + (a+b-1)x + 1}{ax^2 + (-a+b-1)x + 1} \right| \right) \quad (\text{A.2})$$

$$I_3(a, b) = \int_0^1 \frac{dx}{x} \log \left( \left| \frac{-ax^2 + (a+1-b)x + b}{ax^2 + (-a+1-b)x + b} \right| \right) \quad (\text{A.3})$$

$I_1(a, b)$  is the well known function that appears in the calculation of the real part of a triangle diagram. It is possible to perform the integral over the Feynman parameter  $x$ , obtaining the analytical form:



$$I_1(a, b) = \begin{cases} -2 \left( \arctan \frac{1}{\sqrt{b/a-1}} \right)^2 & \text{if } b \geq a \\ \frac{1}{2} \left[ \left( \log \frac{1+\sqrt{1-b/a}}{1-\sqrt{1-b/a}} \right)^2 - \pi^2 \right] & \text{if } b \leq a \end{cases} \quad (\text{A.4})$$

$I_2(a, b)$  and  $I_3(a, b)$  can be expressed in terms of dilogarithms.  $Li_2(x)$  is defined according to Lewin [44]. We find:

$$\begin{aligned} I_2(a, b) = & -Li_2\left(\frac{1-a-b-\sqrt{\Delta_1}}{2}\right) - Li_2\left(\frac{1-a-b+\sqrt{\Delta_1}}{2}\right) \\ & + Li_2\left(\frac{1+a-b-\sqrt{\Delta_2}}{2}\right) + Li_2\left(\frac{1+a-b+\sqrt{\Delta_2}}{2}\right) \end{aligned} \quad (\text{A.5})$$

$$\begin{aligned} I_3(a, b) = & -Li_2\left(\frac{b-a-1-\sqrt{\Delta_1}}{2b}\right) - Li_2\left(\frac{b-a-1+\sqrt{\Delta_1}}{2b}\right) \\ & + Li_2\left(\frac{b+a-1-\sqrt{\Delta_2}}{2b}\right) + Li_2\left(\frac{b+a-1+\sqrt{\Delta_2}}{2b}\right) \end{aligned} \quad (\text{A.6})$$

where we have defined:

$$\Delta_1 = (a+b-1)^2 + 4a, \quad \Delta_2 = (b-a-1)^2 - 4a$$

Let us consider first equation A.5. The second member is explicitly real.  $\forall a, b \geq 0$ , we find that  $\Delta_1 \geq 0$  and that the arguments of the first two dilogarithms  $(1-a-b \pm \sqrt{\Delta_1})/2$  are real and  $\leq 1$ : the corresponding dilogarithms are therefore real. If  $\Delta_2 \geq 0$ ,  $\forall a, b \geq 0$ , the argument of the third and forth dilogarithm  $(1+a-b \pm \sqrt{\Delta_2})/2$  are again real and  $\leq 1$ . If  $\Delta_2 < 0$ , they are complex conjugated and we can use the identity

$$Im(Li_2(z) + Li_2(z^*)) = 0$$

to show that there is no imaginary part. In the latter case it is easier to compute numerically  $I_2(a, b)$  introducing  $Li_2(r, \theta)$ , the real part of the dilogarithm of a complex argument [44]. We rewrite equation A.5 as:

$$\begin{aligned} I_2(a, b) = & -Li_2\left(\frac{1-a-b-\sqrt{\Delta_1}}{2}\right) - Li_2\left(\frac{1-a-b+\sqrt{\Delta_1}}{2}\right) \\ & + 2 Li_2(r(a), \theta(a, b)) \end{aligned} \quad (\text{A.7})$$

where  $r(a) = \sqrt{a}$  and  $\cos \theta(a, b) = (1-a-b)/2\sqrt{a}$ .



It is not necessary to implement numerically equation A.6. Exploiting Landen's functional equation [44]:

$$Li_2(z) + Li_2\left(\frac{-z}{1-z}\right) = -\frac{1}{2} \log^2(1-z)$$

it is possible to express  $I_3(a, b)$  in terms of  $I_2(a, b)$ . We have found the following identity:

$$I_3(a, b) = -I_2(a, b) + \log^2\left(\frac{1+a+b+\sqrt{\Delta_1}}{2\sqrt{b}}\right) - \log^2\left(\frac{1-a+b+\sqrt{\Delta_2}}{2\sqrt{b}}\right) \quad (\text{A.8})$$

For  $\Delta_2 \geq 0$ , the second logarithm squared has a complex argument and takes the form:

$$-\log^2\left(\frac{z}{|z|}\right) = -\log^2\left(\frac{|z| \exp(i\varphi)}{|z|}\right) = \varphi^2$$

where  $\varphi = \arctan((1+b-a)/\sqrt{-\Delta_2})$ .

## References

- [1] G. Jungman, M. Kamionkowski and K. Griest, Phys. Rep. **267** (1996) 195.
- [2] W. L. Freedman, astro-ph/9612024, presented at Conference on Critical Dialogs in Cosmology, Princeton, NJ, 24-27 Jun 1996.
- [3] F. Courbin et al., astro-ph/9705093 (1997).
- [4] A. Dekel, astro-ph/9705033, to appear in the proceedings of the 3rd ESO-VLT Workshop on "Galaxy Scaling Relations: Origins, Evolution and Applications", ed. L. da Costa (Springer-Verlag).
- [5] S. Perlmutter et al., astro-ph/9608192, Astrophys. J., in press (1997).
- [6] C.J. Copi, D.N. Schramm and M.S. Turner, Science **267** (1995) 192.
- [7] E.W. Kolb and M.S. Turner, "The Early Universe", Addison-Wesley (1990).
- [8] F. Zwicky, Helv Phys. Acta **6** (1933) 110.
- [9] L. Bergström and P. Gondolo, Astroparticle Phys. **5** (1996) 183.
- [10] A. Bottino et al., hep-ph/9612451 (1996).
- [11] H.U. Bengtsson, P. Salati and J. Silk, Nucl. Phys. **B346** (1990) 129.
- [12] J. Edsjö and P. Gondolo, Phys. Lett. **B357** (1995) 595; A. Bottino, N. Fornengo, G. Mignola and L. Moscoso, Astropart. Phys. **3** (1995) 65; L. Bergström, J. Edsjö and M. Kamionkowski, astro-ph/9702037, Astrop. Phys. in press (1997).
- [13] L. Bergström, J. Edsjö and P. Gondolo, Phys. Rev. **D55** (1997) 1765.



- [14] T. Gaisser, F. Halzen and T. Stanev, Phys. Rep. **258** (1995) 173, Erratum-ibid. **271** (1996) 355.
- [15] L. Bergström and H. Snellman, Phys. Rev. **D37** (1988) 3737.
- [16] S. Rudaz, Phys. Rev. **D39** (1989) 3549.
- [17] A. Bouquet, P. Salati and J. Silk, Phys. Rev. **D40** (1989) 3168.
- [18] G. F. Giudice and K. Griest, Phys. Rev. **D40** (1989) 2549; L. Bergström, Phys. Lett. **B225** (1989) 372; Nucl. Phys. **B325** (1989) 647.
- [19] M. Urban et al., Phys. Lett. **B293** (1992) 122.
- [20] L. Bergström and J. Kaplan, Astropart. Phys. **2** (1994) 261;
- [21] G. Jungman and M. Kamionkowski, Phys. Rev. **D51** (1995) 3121.
- [22] V. Berezhinsky, A. Bottino and G. Mignola, Phys. Lett. **B325** (1994) 136.
- [23] M.C. Chantell et al., astro-ph/9704037 (1997).
- [24] W.B. Atwood, Nucl. Instrum. Meth. **A342** (1994) 302.
- [25] M. Drees, G. Jungman, M. Kamionkowski and M. Nojiri, Phys. Rev. **D49** (1994) 636.
- [26] S.C. Strausz, Phys. Rev. **D55** (1997) 4566.
- [27] L. Bergström, J. Edsjö, P. Gondolo and P. Ullio, in preparation.
- [28] J.H. Kühn, J. Kaplan and O. Safiani, Nucl. Phys. **B157** (1979) 125.
- [29] K. Fujikawa, Phys. Rev. **D7** (1973) 393.
- [30] J. Edsjö, Aspects of Neutrino Detection of Neutralino Dark Matter (Uppsala University thesis, Uppsala, 1997), hep-ph/9704384.
- [31] H.E. Haber and D. Wyler, Nucl. Phys. **B323** (1989) 267.
- [32] P. Gondolo and G. Gelmini, Nucl. Phys. **B360** (1991) 145.
- [33] M. Drees, M.M. Nojiri, D.P. Roy and Y. Yamada, hep-ph/9701219 (1997).
- [34] J. Edsjö and P. Gondolo, hep-ph/9704361 (1997).
- [35] M.S. Turner, Phys. Rev. **D34** (1986) 1921.
- [36] H.U. Bengtsson, P. Salati and J. Silk, Nucl. Phys. **B346** (1990) 129.
- [37] M. Kamionkowski, proceedings of Les Houches Winter School, France, 1994.
- [38] J.R. Ipser and p. Sikivie, Phys. Rev. **D35** (1987) 3695.
- [39] V.S. Berezhinsky, A.V. Gurevich and K.P. Zybin, Phys. Lett. **B294** (1992) 221.
- [40] M. Urban et al., Talk presented at the International Conference on Cosmic Ray Physics, Calgary (July 1993).



- [41] J. Silk and A. Stebbins, *Astrophys. J.* **441** (1993) 439.
- [42] R. Ibata, G. Gilmore and M. Irwin, *MNRAS* **277** (1995) 781.
- [43] A. Bottino, C. Favero, N. Fornengo and G. Mignola, *Astrp. Phys.* **3** (1995) 77.
- [44] *Structural Properties of Polylogarithms*, L. Lewin Editor (American Mathematical Society, Providence, 1991).



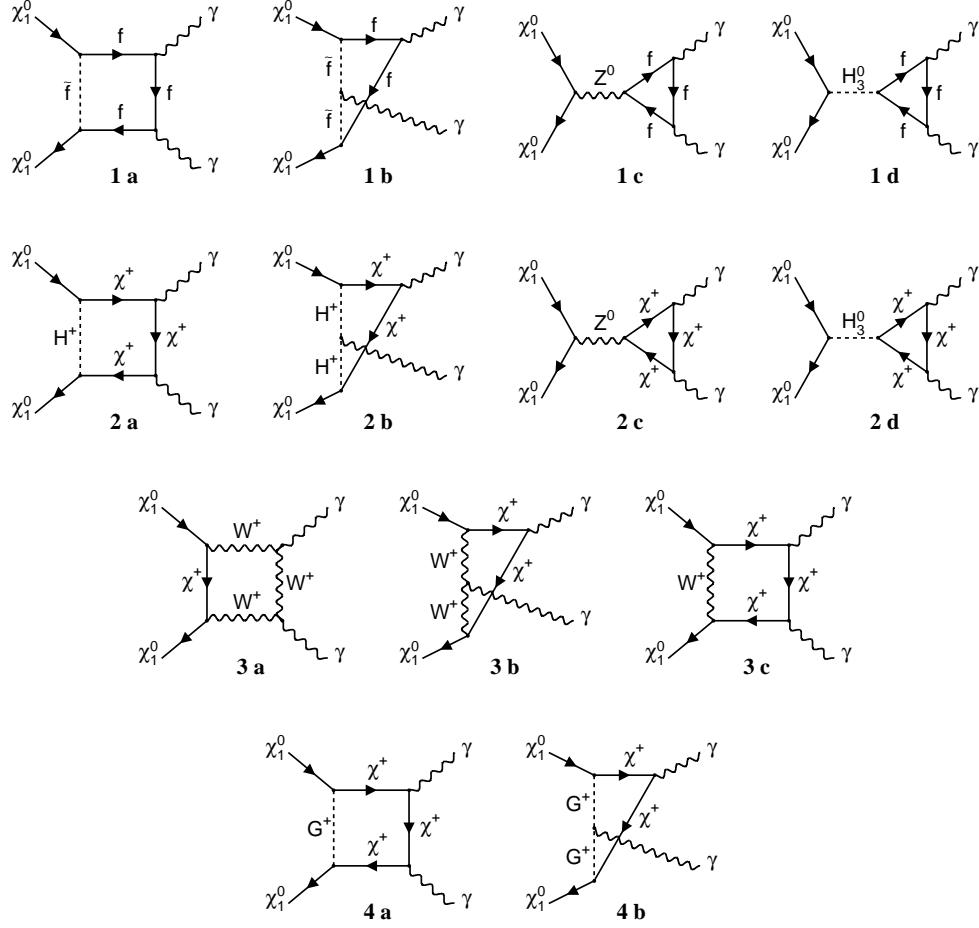


Figure 1: Feynman diagrams contributing, at one loop level, to neutralino annihilation into two photons. Diagrams with exchanged initial and final states are not shown.



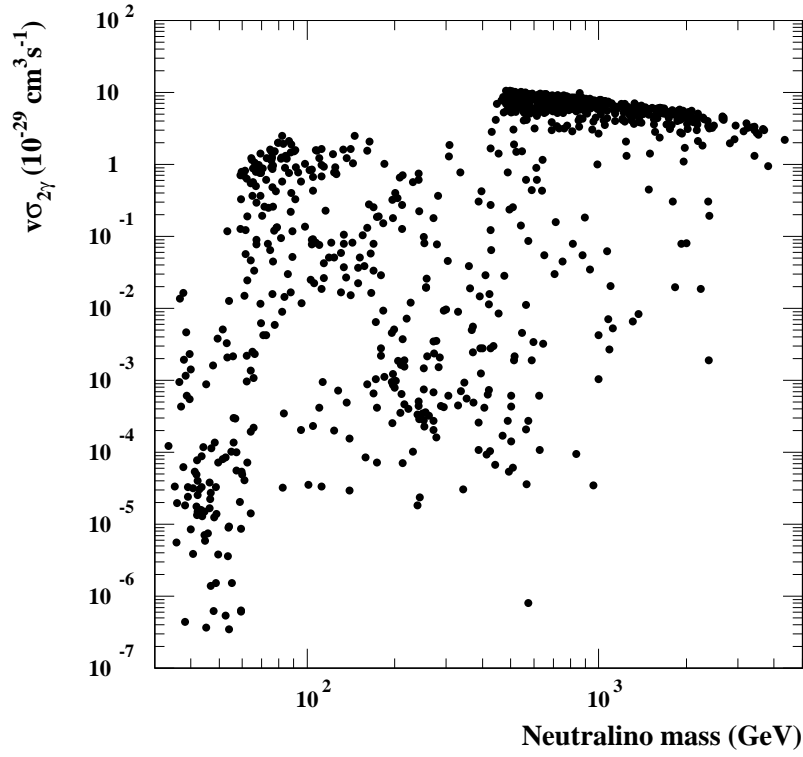


Figure 2: Annihilation rate of neutralinos into  $2 \gamma$  for a broad scan in supersymmetric parameter space (the parameter range is identical to that of the “generous scan” of Table 2.2 in [34,30]).



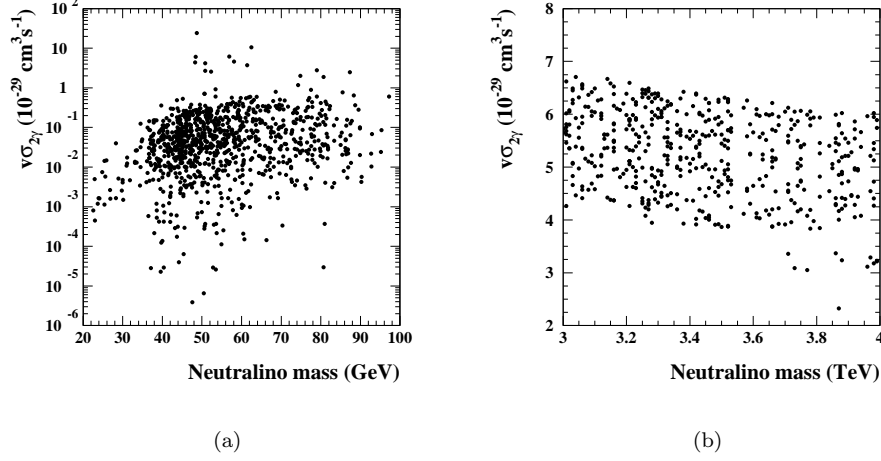


Figure 3: Annihilation rate of neutralinos into  $2\gamma$  for more extensive scans in the low- and high-mass regions.

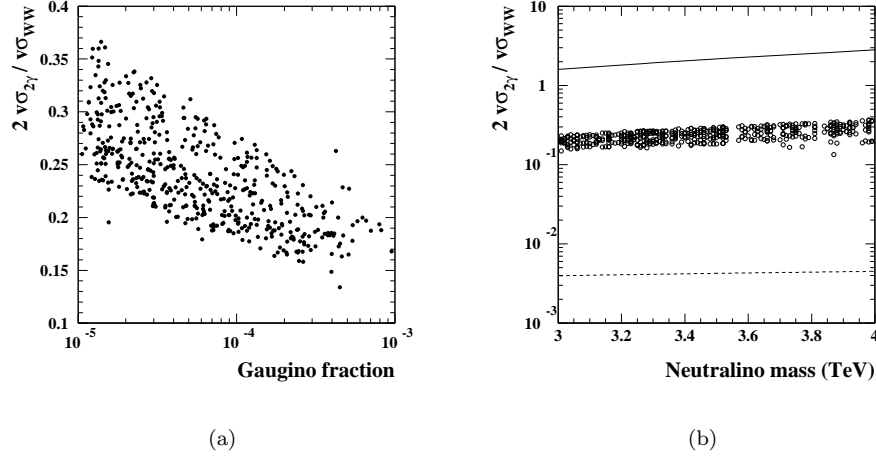


Figure 4: In Fig. (a) ratio  $2v\sigma_{2\gamma}/v\sigma_{WW}$  as a function of the gaugino fraction  $Z_g$ ; in Fig. (b) ratio  $2v\sigma_{2\gamma}/v\sigma_{WW}$  for the sampled supersymmetric models of Fig. (a), the unitarity lower bound of [20] (dashed line) and the pure higgsino rate obtained in this work (solid line).



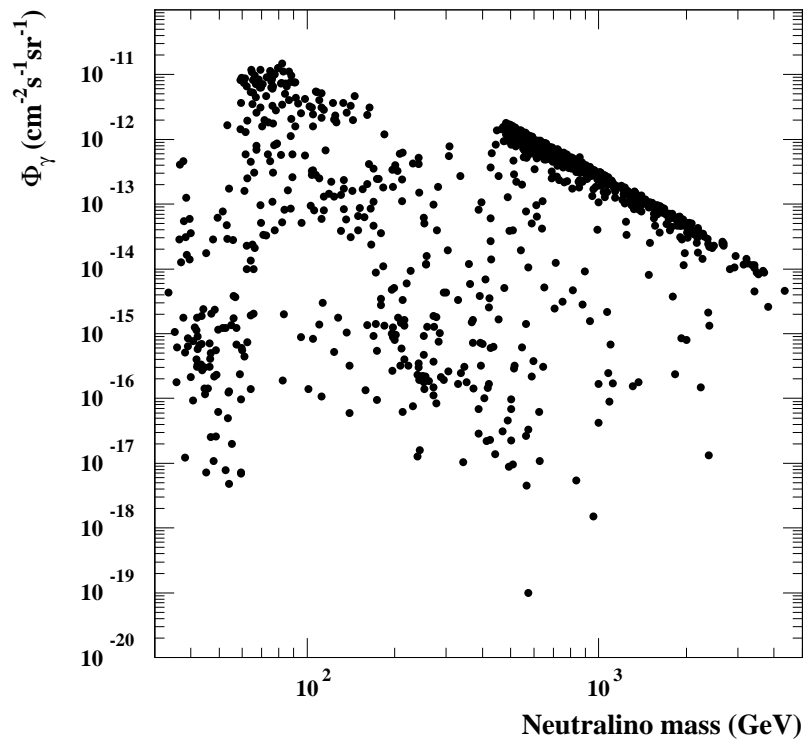


Figure 5: Normalized flux  $\Phi_\gamma$  for the same models as those in Fig. 2.



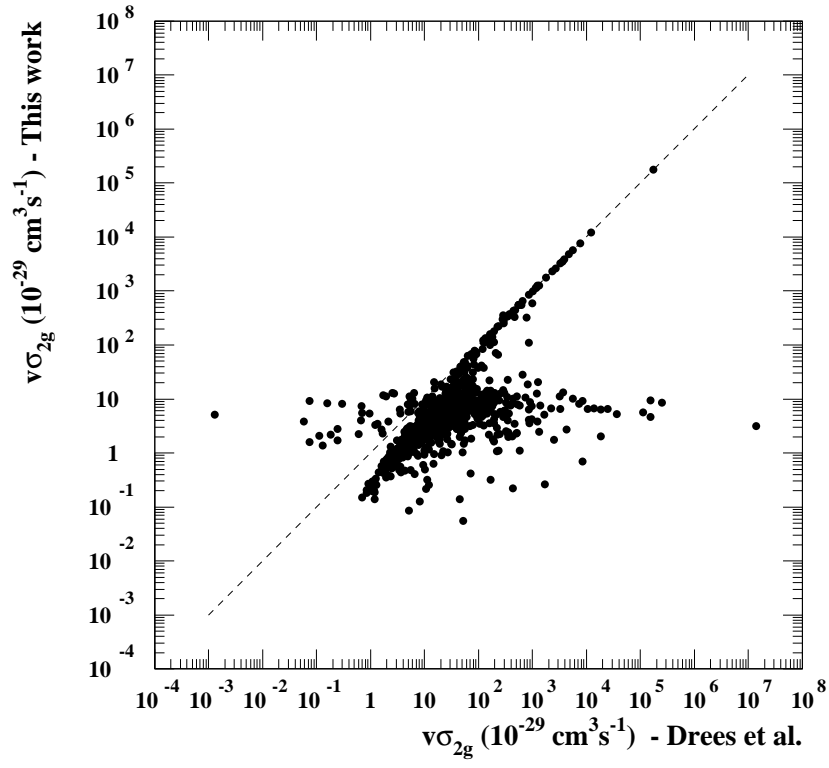


Figure 6: Value of  $v\sigma_{2g}$  for a scan of low-mass neutralino models using our results compared to the value obtained with previous formulas [25].